

# Laboratory tests to determine the critical shear stress of frozen and thawed soils



**JULIE MALENFANT LEPAGE**

Researcher/PhD Candidate  
NTNU/Laval University  
[julie.m.lepage@ntnu.no](mailto:julie.m.lepage@ntnu.no)

 **NTNU**  
Norwegian University of  
Science and Technology

 **UNIVERSITÉ  
LAVAL**

# 1. Introduction

Climate change contributes to many perturbations in Northern countries. It has been proven that northern latitude countries are more affected by temperature raise, especially during the winter season. Changes in the hydric regime is to be foreseen. The increase in rainfalls during winter coupled with the increase of extreme weather events will have a negative effect on natural sediment deposits. Landslide, gully erosion, degradation of roads and railways embankments, failure of drainage systems are just a few challenges awaiting Norway in a changing climate perspective.

Sediment motion initiation has been extensively studied for over a century (Guo, 2020), but the erodibility potential of frozen ( $< -2^{\circ}\text{C}$ ) and partially frozen soils (0 to  $-2^{\circ}\text{C}$ ) is still poorly understood and less documented in the literature. It has been generally accepted in cold region areas that only thawed soils can be removed from the substrate by water. However, with a certain amount of unfrozen water content within a frozen soil, single grains should be able to be detached and transported (Guegan, 2016).

A problem that arises when we look at erosion of frozen soils is the determination of the critical shear stress (characterised by the abbreviations  $\tau_c$  or CSS). It is a fundamental parameter for assessing the erodibility potential of a soil and is defined as the shear stress generated on the soil surface by water flow at which significant erosion is initiated (Figure 1). The critical shear stress is widely use in sediment transport models as well as for calculations of soil erosion rates. This research project aims to use a cohesive strength meter (CSM) to assess the CSS of frozen silts in the laboratory. To our knowledge, the CSS of a frozen silt has never been measured under different sub-zero temperatures. To achieve this, an international research collaboration was established between the Sustainable Arctic Marine and Coastal Technology research program (SAMCoT) from the Norwegian University of Science and Technology (NTNU) in Trondheim, Norway and the Arquluk and Sentinel North research programs from Université Laval in Québec, Canada.

It is expected that the erosion potential of a soil will change as temperature decreases and under different degree of consolidation. As part of this study, the temperature of the silt samples varied between  $-6$  and  $+2^{\circ}\text{C}$  and two levels of consolidation were applied, i.e. 10 and 50 kPa. The laboratory testing setup was established at the Department of civil and environmental engineering at NTNU. In total, more than 35 erosion tests were carried out. The state of

knowledge on erosion of frozen soils, the methodology developed with the CSM, and the results obtained in this study are presented in the following sections.

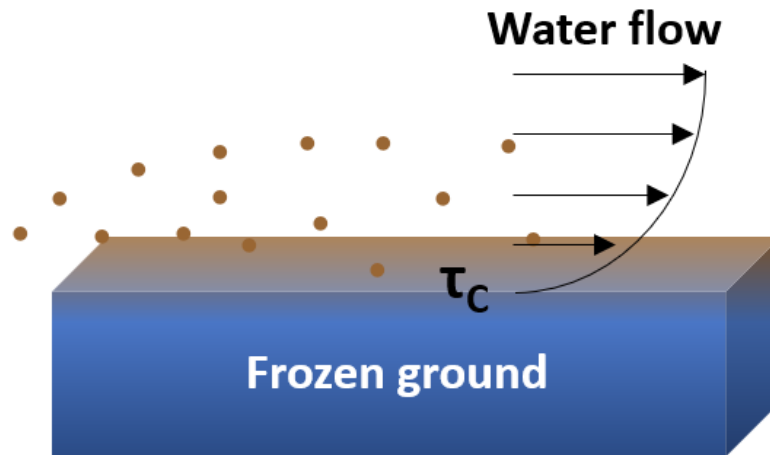


Figure 1: Surface erosion caused by moving water.

## 2. Critical shear stress of seasonally frozen soils

To quantify the erosion potential of soils, two parameters are typically used: the critical shear stress ( $\tau_c$ ) and the erosion rate ( $\varepsilon$ ) which is the mass or volume of sediment eroded per unit time once the erosion threshold  $\tau_c$  is exceeded. The rate of erosion is often expressed by the following relationship:

$$\varepsilon = k(\tau_e - \tau_c) \quad (1)$$

Where  $k$  is the erodibility or detachment coefficient and  $\tau_e$  is the effective flow stress. For instance, a high erosion potential corresponds to a less stable soil matrix having a lower critical shear stress combined with a great erodibility coefficient. Within the framework of this research, the determination of the critical shear stress is the main focus.

Some researchers have observed that riverbank erosion rates were highest during the winter and thawing periods, and that frost action was playing a fundamental role in the erosion process (Wolman 1959, Lawler 1986, Lawler 1992, Stott 1997, Yumoto 2006, McCool et al. 2013). Rain or snowmelt on frozen ground is often the main cause of severe runoff and erosion events (Zuzel et al. 1982; Yen and Molnau 1982, Flerchinger et al. 2013). Ice seal soil particles as the ground freezes which greatly diminish the permeability of the soil, prevent water infiltration,

increase runoff rates, and subsequently soil loss (Zuzel et al. 1982, Froese et al. 1999, Flerchinger et al. 2013). In addition, Leopold (1973) suggested that for effective riverbank erosion to occur, the material must be loosened which can be done by the formation of ice crystals in winter. Freezing also causes water migration to the freezing front which locally increase moisture content while decreasing the soil density and making it more susceptible to fluvial entrainment (Flerchinger et al. 2013, Guegan, 2016).

In areas experiencing seasonal frost, it was also found that freeze-thaw is a dynamic process affecting soil stability and its resistance to flowing water. Studies showed that freeze-thaw increase soil porosity by pushing soil particles apart when water turns into ice, reduce soil bulk density, change moisture content, decrease soil strength, soil particles cohesion and penetration resistance (Liu et al. 2017, Sun et al. 2021). It was observed that freeze-thaw cycles were of much greater importance in controlling erosion from till banks consisting of fine clays than those made of coarser material (Hill 1973 in Henshaw et al. 2012). This correlates well with the fact that fine-grained soils are more frost susceptible. Ferrick and Gatto (2005) demonstrated that the erodibility of silty soils with high moisture content increased significantly during runoff events following thaw.

Some research works have quantified the impacts of freeze thaw cycles on soil erodibility especially for agriculture soils. Edwards and Burney (1987) observed that freezing followed by thawing of a bare soil significantly increased sediment loss by about 90%. Through CT scanning and digital image processing technology, Jiang et al. (2019) showed the weakening of soil structure after a different number of freeze-thaw cycles. The soil porosity did increase from 7.8% to 23.34 % after 20 freeze-thaw cycles (Figure 2). Liu et al. 2017 tested a typical black soil from Northeast China under different number of freeze-thaw cycles (0, 1, 3, 5 and 10 cycles) and four gravimetric moisture contents (10, 20, 30 and 45%). They found out that freeze-thaw processes can change soil properties and generally increased soil detachment capacity by an average of 36.5%. The CSS measured after thawing were highest (4.01 Pa) and lowest (1.81 Pa) both after 10 freeze thaw cycles, but respectively at 20% and 45% moisture content. According to them, alternating freeze-thaw seem to increase the stability of soil aggregates at an intermediate water content and decrease the stability at either lower or higher moisture contents.

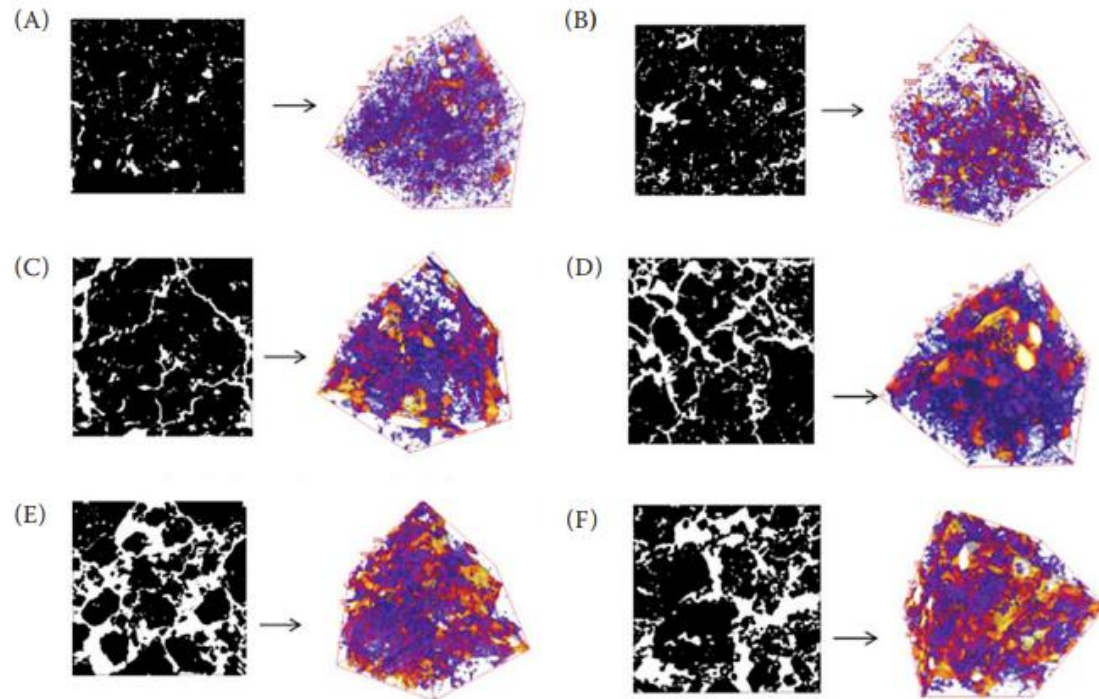


Figure 2: 2D and 3D visualisations of the soil structures under different freeze-thaw cycles: (A) before the freeze-thaw; (B) after the first freeze-thaw cycle; (C) after 5 freeze-thaw cycles; (D) after 10 freeze-thaw cycles; (E) after 15 freeze-thaw cycles; and (F) after 20 freeze-thaw cycles. On the 2D images, the white part corresponds to the pores and the black part to the soil. On the 3D images, the yellow part corresponds to the pores present at the edges of the cubes and the purple part to the inner pores (Jiang et al. 2019 In Sun et al. 2021).

McCool et al. (2013) did experiments on bare tilled fallow runoffs plots where erosion events were categorized into summer events, winter events on frozen soil, winter events on thawing soil, and winter events on non-frozen or thawed soil. Thawing soil was found to be the most erodible with the lowest  $\tau_c$  and highest rill soil erodibility factor  $k_r$  while frozen soil was the least erodible, with a relatively high  $\tau_c$  and the lowest  $k_r$  value. Non-frozen or thawed soil in winter had lower  $\tau_c$  and  $k_r$  values than the soil in summer but the authors suggested that the overall erosion may not differ.

To conclude, soil erosion mechanism of seasonally frozen soils is clearly different from non-frozen soils since phase change of water is the main factor controlling soil properties under freeze-thaw conditions. Quantitative relationships between the soil erodibility and soil properties have seldom been assessed under different freeze thaw conditions (Sun et al. 2021) and neither the CSS values. According to Van Klaveren and McCool (2010), erosion models should have a winter component that considerer the transient effects of freeze-thaw.

### **3. Cohesive Strength Meter: Applicability to frozen soils**

This research project aims to measure critical shear stress of frozen and partially frozen soils. To do so, an in-situ erosion device developed for cohesive soils, the cohesive strength meter CSM, was used and adapted for tests on frozen soils. The CSM is the only erosion apparatus that is commercially available, making it more readily accessible to researchers (Grabowski et al. 2010). It offers also other advantages: it is a lightweight and compact portable device, the set up is quick to do, operations to follow are simple, the measurement time is rapid (less than 5 min per erosion test) and subsequently many replicates can be taken quickly. Since its conception 40 years ago (Paterson 1989), the CSM has been increasingly used to measure spatial and temporal variations in erosion threshold for fine-grained sediments, particularly in estuarine and intertidal environments (Yallop et al. 1994, Tolhurst et al., 1999; Yallop et al., 2000; Friend et al., 2005; Widdows et al. 2007) but more recently in rivers (Grabowski et al., 2010, Grabowski et al., 2012) and terrestrial environments (Aviles et al. 2020). The CSM is made of an operating panel, a water reservoir pressurized by an external air cylinder, an analogue pressure gauge and a sensor head (Figure 3A and 3B). Inside the sensor head there is a jet nozzle firing water at different pressures. An optical sensor that determines sediment resuspension by using attenuation of an infrared light path is also present within the test chamber at 1 cm below the jet nozzle (Figure 3C). The repeatability of the light source is +/- 0.015% FSD (full scale deflection). The CSM records the internal jet pressure for each step in PSI.

The Cohesive Strength Meter MK IV from the manufacturer PARTRAC offers forty-two predefined routines having different: pressure increment between water jets, maximum pressure reached at the end of a test (up to 60 PSI), jet duration, time between jets and light transmission logging duration. The choice of routine should be based on the erosion resistance of the sediment. For example, for sediment of low resistance the pressure steps should be small with long intervals between water jets, whereas for sediment of higher resistance, the change in pressure should be larger and the intervals shorter (Vardy et al. 2007). Finally, the erosion threshold is defined by the manufacturer (PARTRAC) as the jet pressure at which average light transmission at 1cm above the sediment surface drops by 10% below the maximum.

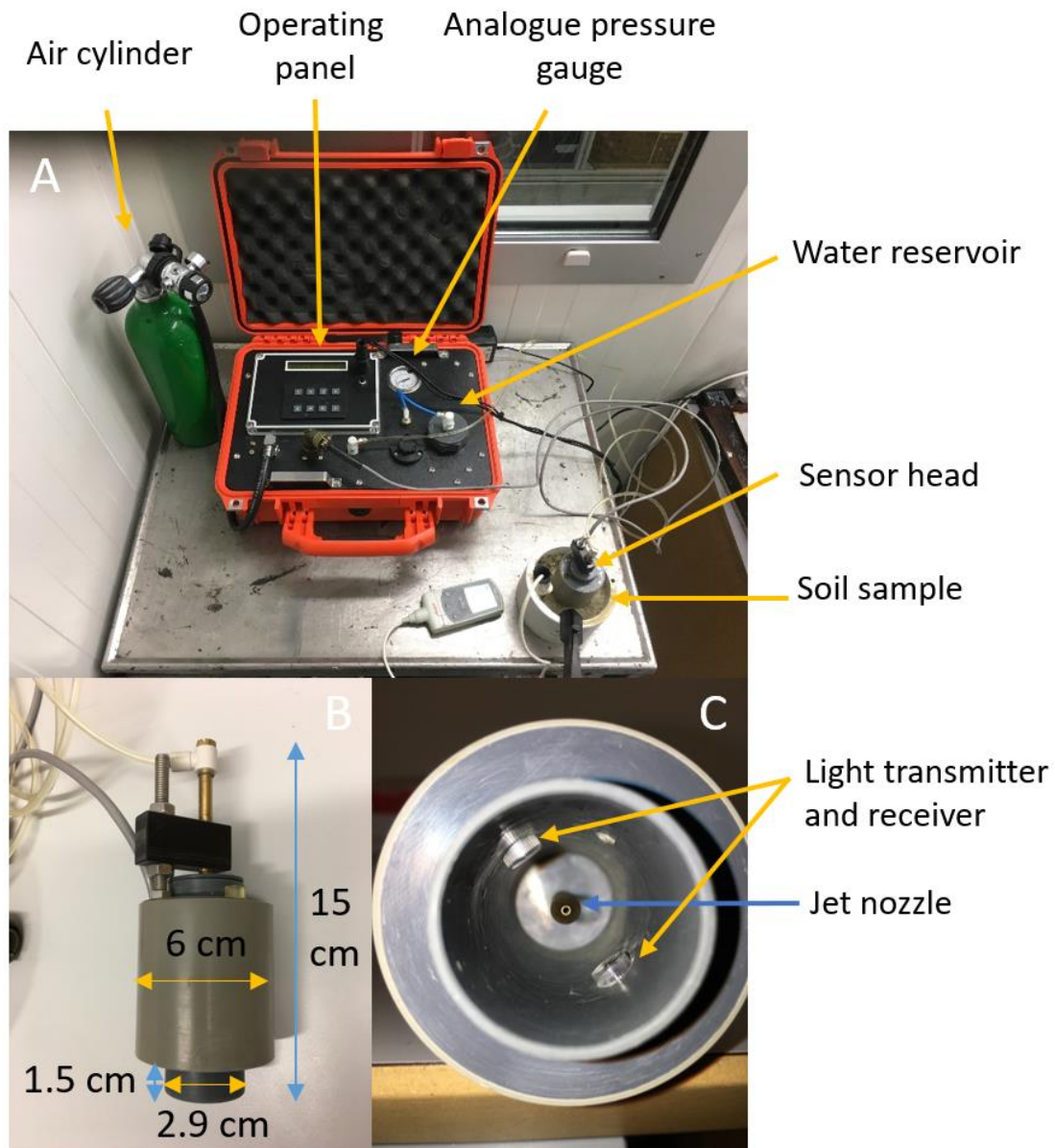


Figure 3: A) The Cohesive Strength Meter MK IV from Partrac; B) the sensor head assembly and C) the jet nozzle, the light transmitter and receiver.

### 3.1 Laboratory methodology

Since the CSM has never been applied on frozen soils, a methodology of used has been developed in the laboratory as part of this research. The laboratory work is divided into three distinct stages: 1) characterization of the soil to determine relevant geotechnic parameters, 2) soil consolidation and freezing and 3) testing with the CSM in a cold room.

### 3.1.1 Soil characterization

Silt is considered to have one of the highest sensitivities to erosion and was chosen as part of this study. The silt used comes from an experimental road site built by NTNU in 2016 and located south-west of the town of Røros in Norway (Loranger 2020). The soil was sieved to remove the bigger particles from the fine matrix and to obtain a more homogeneous soil. Only the particle size ranges smaller than 1 mm were kept for the experimentation. Figure 4 shows the soil grading curve done with a PARIO automated hydrometer having an estimated error of +/- 0.5%.

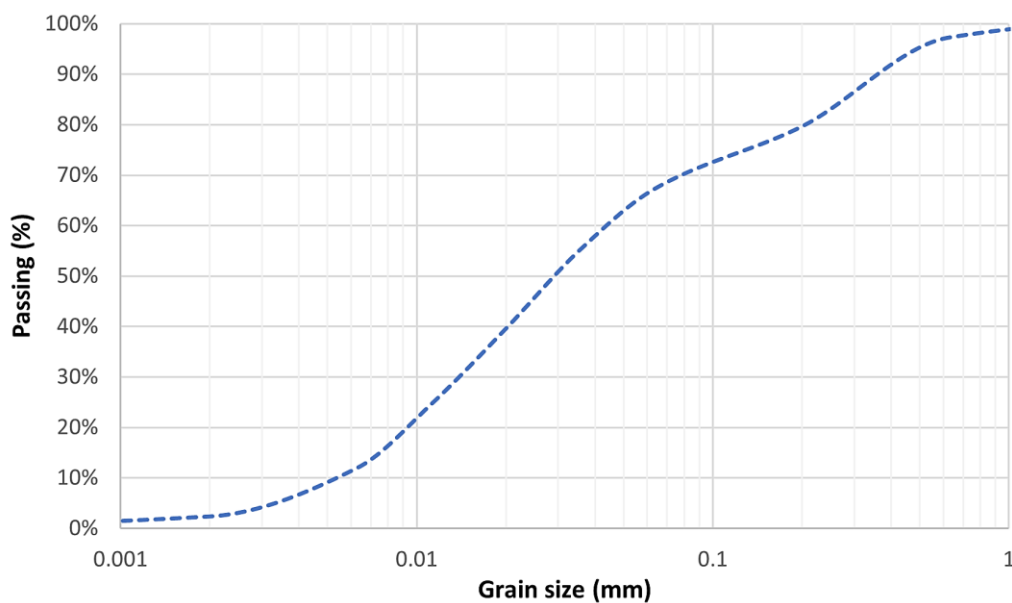


Figure 4: Grain size distribution curve of the soil used in this study

From the grain size distribution, a median grain size  $d_{50}$  of 0.029 mm was obtained. The PARIO uses the USDA soil classification which tell us that the soil sample consist of 2% clay, 61% silt and 37% (Figure 5) while the USCS soil classification give us respectively 2% clay, 68% silt and 30% sand. The soil is thus classified as a silt loam according to the soil texture triangle of Figure 6 (see orange dot). The particle density  $\rho_s$  of the soil is 2700 kg/m<sup>3</sup> and was acquired by following these standards (Handbook R210 (213); ASTM D854). A saturated water content of 25.7% was calculated for this soil.

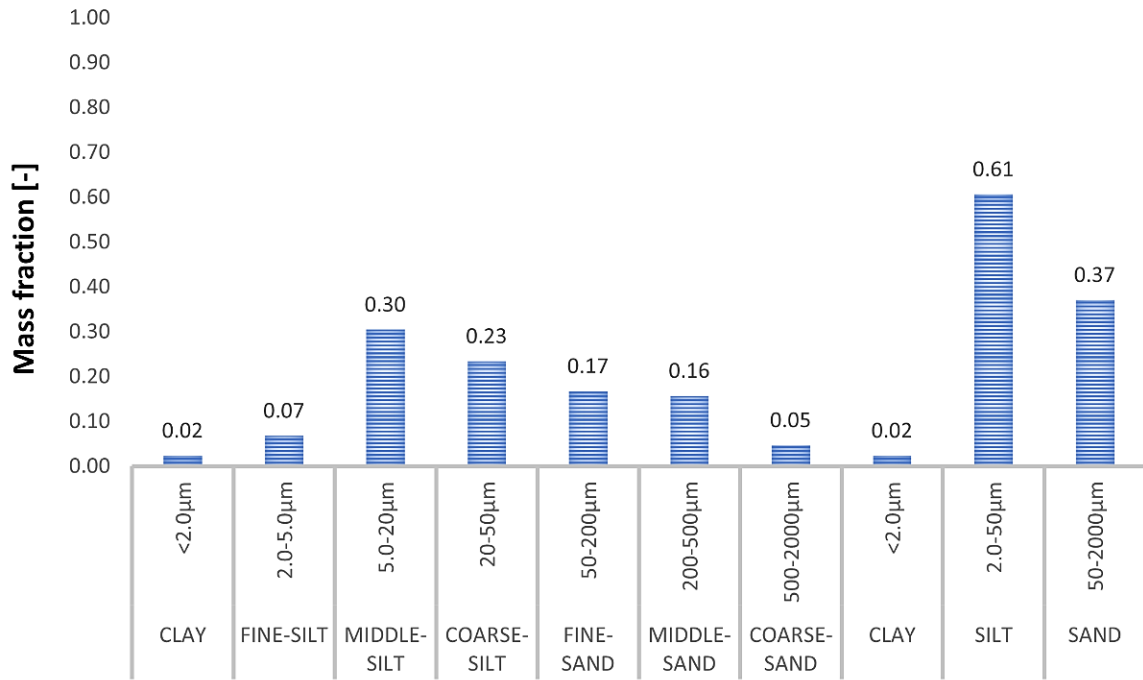


Figure 5: Mass fraction of different texture classes (USDA soil classification)



PARIO

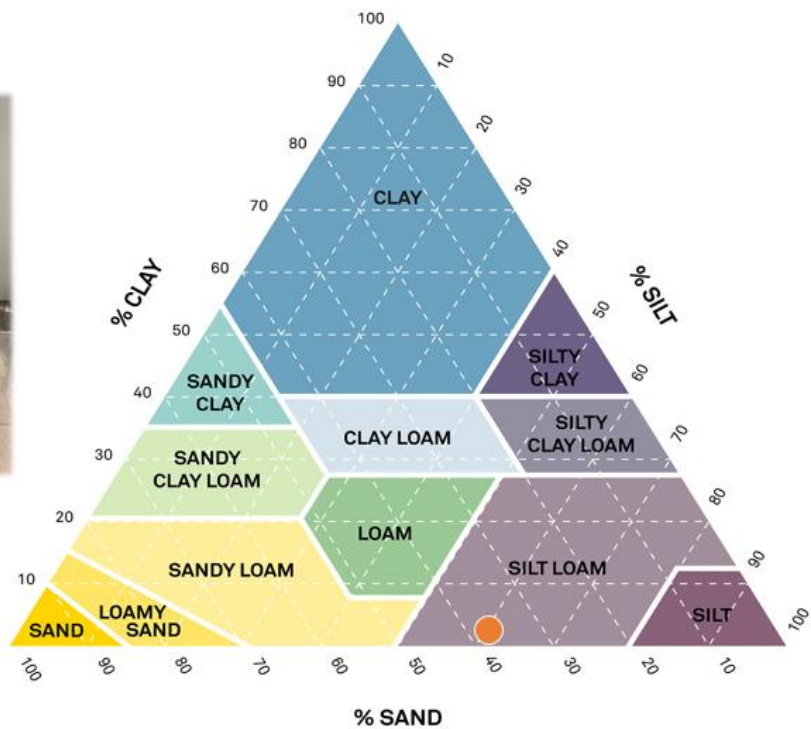


Figure 6: Classification of the soil type according to the soil triangle of the US Soil Taxonomy

### 3.1.2 Soil consolidation and freezing

Consolidation molds large enough to hold the sensor head of the Cohesive Strength Meter were made at NTNU (Figure 7A). The inner ring has a diameter of 99.6 mm and a height of 50 mm (Figure 7B). To evaluate the potential effect of soil consolidation over critical shear stress, 730 g of saturated soil was added in each mold and consolidated either at 10 or 50 kPa with an oedometer (Figure 7C). The soil samples were consolidated overnight, and two-ways drainage was allowed through porous disks located at the top and the bottom of the mold. Once consolidated, the soil samples were placed in a cooling box at the desired freezing temperature. The outer of the molds was covered with mineral wool to encourage unidirectional freezing from the top.



Figure 7: Laboratory set up: A) Compaction mold made at NTNU; B) Schematic of the mold with dimensions; C) Oedometers used.

### 3.1.3 Testing with the Cohesive Strength Meter

Testing with the CSM was done in a cold room at a temperature of +2°C to simulate spring conditions where cold water is flowing over frozen ground. The water in the CSM reservoir was thus kept at +2°C during all the tests done. For the unfrozen soil samples, the sensor head was simply pushed 1.5 cm deep into the soil, up to the lower flat edge of the sensor head (Figure 8A). Once inserted, the jet nozzle is located 2 cm above the soil surface. For the frozen soil samples, a 32 mm hole saw was used to drill the circumference of a circle in order to insert the sensor head (Figure 8B). The area of sediment tested is 6.6 cm<sup>2</sup>. Afterwards, by using a syringe, the sensor head was filled very carefully with water at +2°C through the small tube located at the top of the sensor (Figure 8C). The value of the light transmission inside the sensor is given by the CSM after this procedure. However, on muddy soils, some minimal erosion is unavoidable during filling and a starting transmission of 100% is often not attainable (PARTRAC, 2011). A transmission reading smaller than 70% is considered to reduce the resolution of a test and hence the quality of the data. For this reason, only tests having a starting light transmission between 70 and 100% were considered in this study and were thereafter normalized.

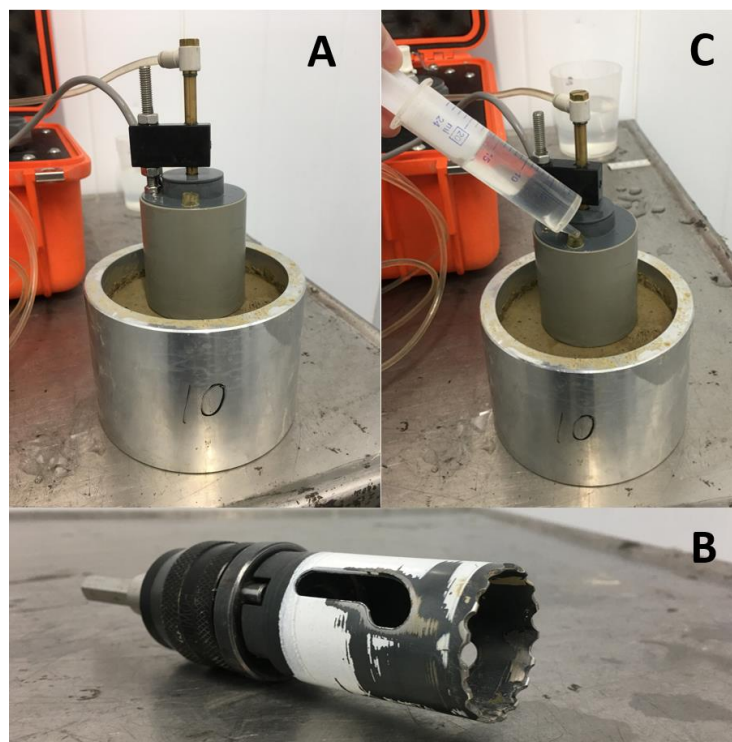


Figure 8: A) Sensor head inserted into a soil sample; B) Hole saw used to drill in frozen soil samples; and C) Water filling of the sensor head with a syringe.

The CSM routine SAND 1 was used for all erosion tests to be able to later apply the methodology developed by Grabowski et al. in 2010 to estimate critical shear stress (see section 3.2.2). This routine has the following characteristics: a low initial jet pressure of 0.3 PSI, a short jet duration of 0.3 seconds followed by 3 seconds of data logging, pressure increments of 0.3 PSI and a maximum jet pressure of 12 PSI (Figure 9). During the test duration of 2 minutes, a total of 40 water jets were fired on the sediment surface.

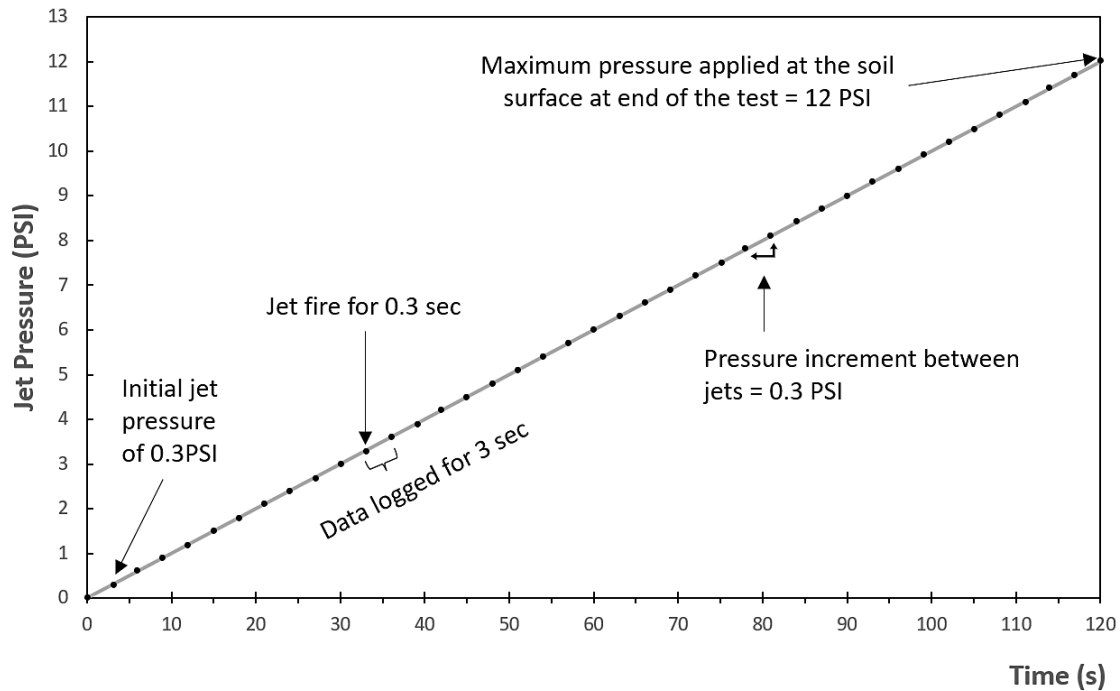


Figure 9: Schema explaining the routine SAND 1 of the Cohesive Strength Meter MK IV.

The soil surface temperature of the samples was taken at the start of each erosion test with a high precision thermometer TFX 444 having an accuracy of  $\pm 0.3^{\circ}\text{C}$ . Once the CSM routine ended, the erosion scours dimensions left on the soil surface were also measured.

During data analysis, after each fired water jet, the light transmission is averaged for 1 second of data logged (i.e from the 2<sup>nd</sup> to the 12<sup>th</sup> values). Figure 10 shows an example of erosion profile obtained for a soil sample frozen at  $-3.1^{\circ}\text{C}$  where the jet pressure is plotted against the average light transmission. Erosion profiles can be divided in three distinctive sections (Tolhurst et al. 1999). Part A is usually quite horizontal with average transmission values near 100%. However, in some cases the light transmission is lower at the start of the test and slowly increase after the first jets of water. Part B shows the drop in light transmission as erosion occurs within the sensor head. The erosion threshold is found at the pressure step at which transmission drops by 10% from values in Part A. On Figure 10, the erosion threshold occurred

at 2.9 PSI. Finally, part C is where the profile is asymptotic. Light transmission values tend towards zero as the applied jet pressure increases and the concentration of suspended sediment is highest.

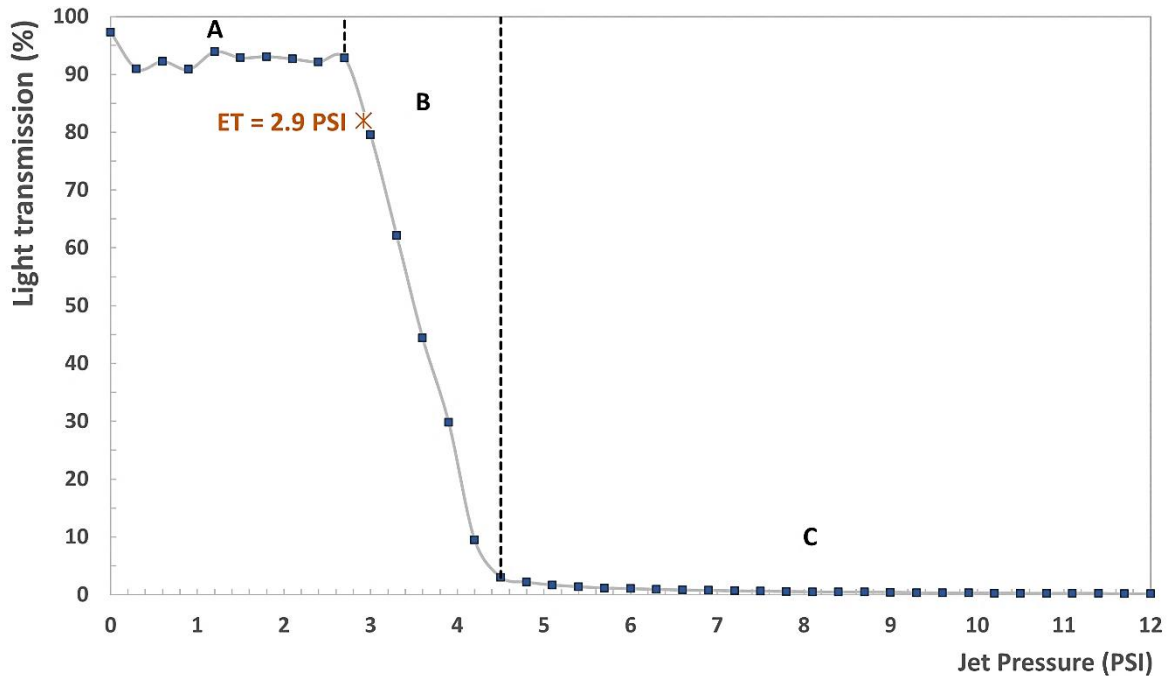


Figure 10: Example of an erosion profile obtained with a CSM for a frozen sample (-3.1°C). The erosion threshold (ET) is occurring at a jet pressure of 2.9 PSI.

### 3.2 Conversion of the vertical jet pressures measured into horizontal bed shear stresses

#### 3.2.1 Step 1: Calibration method proposed by Vardy et al. (2007) to obtain pressures applied at the sediment surface

Since the CSM device records vertical exit jet pressures, there was a need to transpose these pressures into equivalent horizontal hydraulic forces since critical shear stresses are input parameters commonly used in sediment transport models. The first of two required steps to achieve this was proposed by Vardy et al. (2007). They suggested that each CSM device should be calibrated so that the actual flux of the jet is rather express as a pressure directly applied on the surface sediment. This pressure is termed stagnation pressure  $P_{stag}$  with units in Pascal and can be obtained from Equation 2 (Vardy et al. 2007). It was found that comparing results of  $P_{stag}$  between different CSM units and models was more accurate due to the constructional variations that exist between devices.

$$P_{stag} = \frac{1p_w(7)^24Q^2}{2d^2(z - z_0)^2\pi} \text{ for } z > z_0 \quad (2)$$

In Equation 2,  $p_w$  is the density of water ( $\text{kg/m}^3$ ),  $Q$  is the flux of the jet ( $\text{m}^3/\text{s}$ ),  $d$  is the jet orifice diameter (m),  $z$  is the vertical distance between the jet and the sediment surface (m) and  $z_0$  is the virtual origin of the jet (m). More specifically  $z_0$  is the limit between the zone end of flow establishment and the beginning of the established flow zone (Figure 11) where the water from the jet starts mixing with the water in the sensor head. Lee and Chu (2003) proposed, for a round turbulent jet, a  $z_0$  equivalent to 6.2 times the jet orifice diameter.

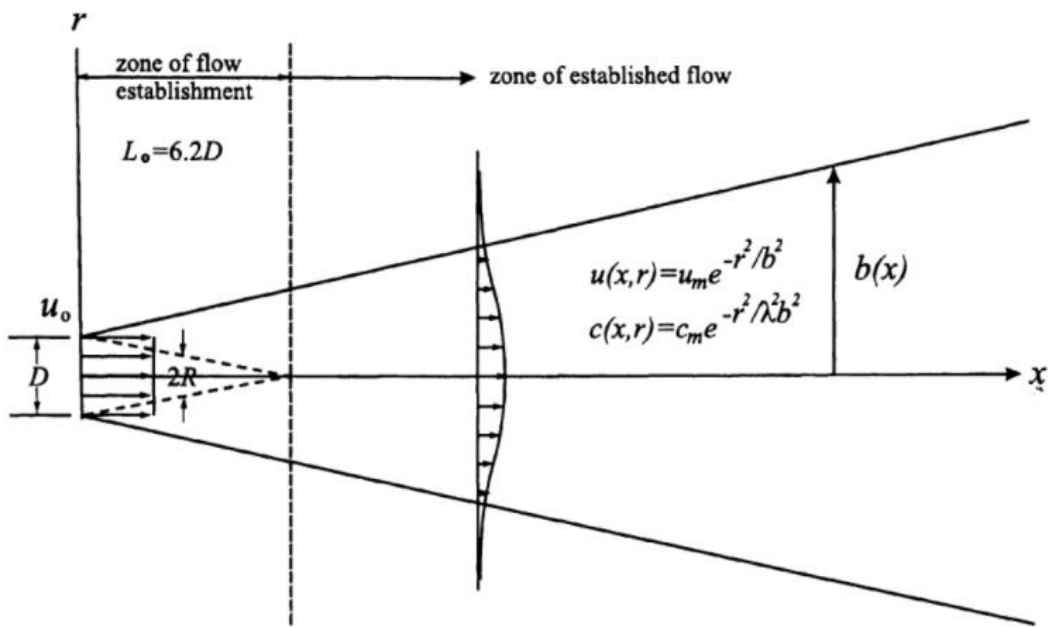


Figure 11: Flow from a round turbulent jet (Lee and Chu, 2003)

To obtain the jet flow  $Q$ , the amount of water released by each jet during the first half of routine SAND 1 (i.e., from 0.3 to 6 PSI) was collected in plastic cups (Figure 12), then weighed, converted into a volume of water, and divided by a jet pulse time of 0.3 seconds. This step was done 5 times. It was estimated that the erosion threshold would be reached at low jet pressures for the soil tested, which explains why the CMS calibration was not carried out for pressures higher than 6 PSI. Here is an example of  $P_{stag}$  calculation for a jet pressure of 2.1 PSI.

$$P_{stag} = \frac{98 \times 1000 \text{ kg/m}^3 \times (1.3 \times 10^{-6} \text{ m}^3/\text{s})^2}{(0.0011\text{m})^2 \times (0.02\text{m} - (6.2 * 0.0011))^2 \times \pi} = 236.8 \text{ Pa}$$

All values of the calibration process for the first 20 jets of routine SAND1 are presented in Table 1. Figure 13 shows the relation between jet pressures and values of calculated Pstag. Irregular stagnation pressures are observed respectively at 0.9, 1.2, 2.4, 5.1 and 5.4 PSI and are likely to be caused by anomalous water fluxes. Vardy et al. (2007) examined in more details firing duration of jets of routines SAND 3 and SAND 9. They observed that most of the jet durations were as programmed but several were shorter or longer, meaning for instance that shorter jet durations resulted in lower water fluxes and thus lower stagnation pressures. Therefore, these anomalous values were removed from the data set, and the new relationship given by Equation 3 was used as calibration equation as part of the data analysis of this study.

$$P_{stag} = 94.06x^{1.18} \text{ for } x < 6\text{PSI} \quad (R^2 = 0.99) \quad (3)$$

Table 1: Mean weight of water released, mean flow and calculated stagnation pressure  $P_{stag}$  for the first 20 jets of SAND 1 routine

Jet pressure (PSI)	Water (g)	Jet flow (m <sup>3</sup> /s)	Pstag (Pa)
0.3	0.11	3.5E-07	18.8
0.6	0.20	6.5E-07	64.6
0.9	0.31	1.0E-06	162.7
1.2	0.17	5.8E-07	51.8
1.5	0.28	9.4E-07	134.6
1.8	0.35	1.2E-06	203.6
2.1	0.37	1.2E-06	236.8
2.4	0.47	1.6E-06	370.6
2.7	0.43	1.4E-06	314.3
3	0.46	1.5E-06	359.9
3.3	0.48	1.6E-06	392.1
3.6	0.51	1.7E-06	433.6
3.9	0.55	1.8E-06	507.9
4.2	0.54	1.8E-06	490.6
4.5	0.57	1.9E-06	549.9
4.8	0.58	1.9E-06	566.3
5.1	0.77	2.6E-06	994.0
5.4	0.46	1.5E-06	357.7
5.7	0.65	2.2E-06	708.2
6	0.66	2.2E-06	747.8



Figure 12: Calibration of the CSM

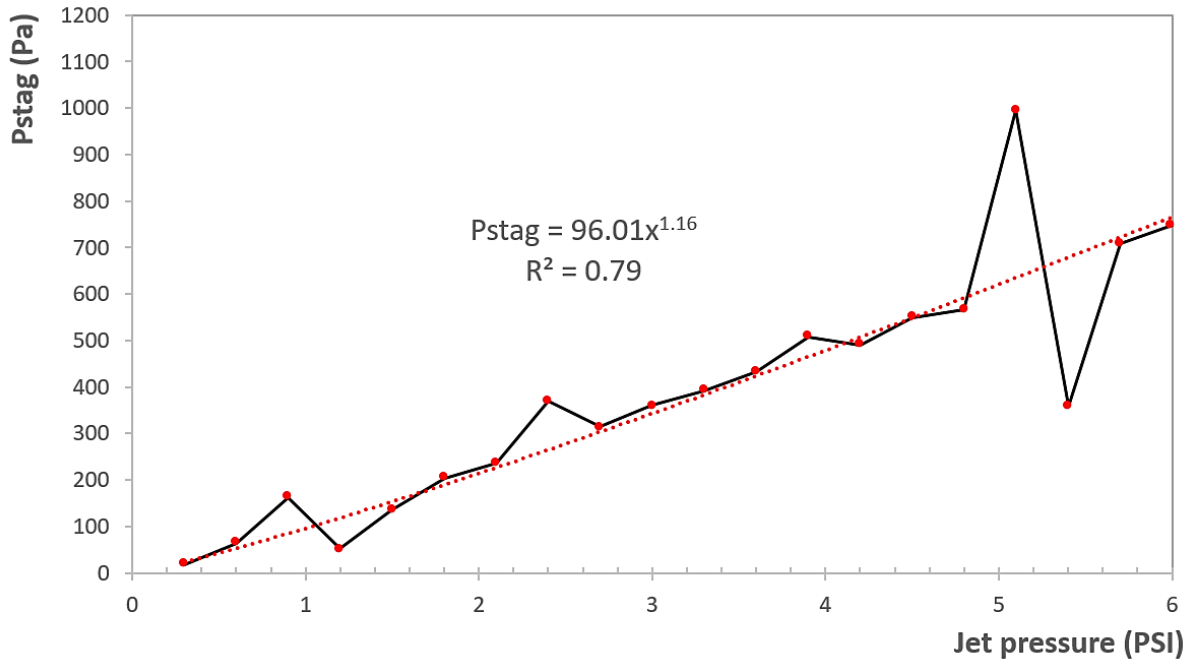


Figure 13: Stagnation pressures ( $P_{stag}$ ) on the soil surface for the first 20 water jets of routine SAND 1

Figure 14 shows a strong correlation between Equation 3 and the calibration equation published by Vardy et al. 2007 for the CSM Mark IV<sub>hp</sub>. It can also be observed that the difference between the blue (with data removed) and the red (with all data) curves is very slight.

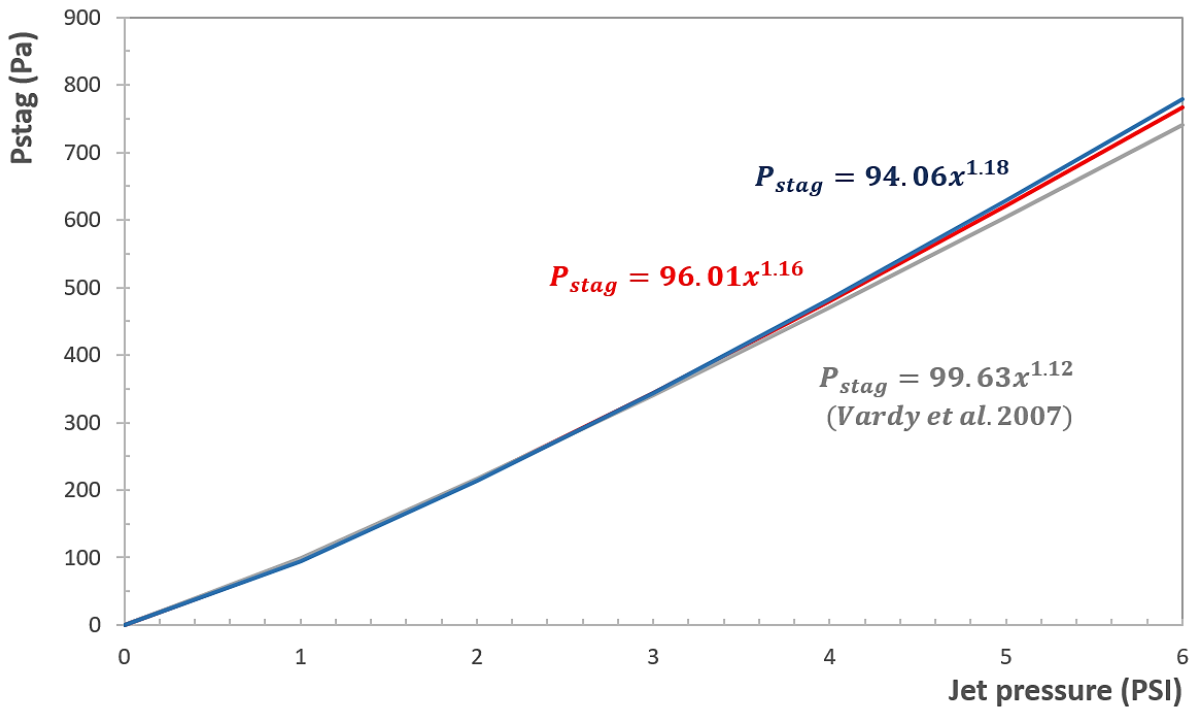


Figure 14: Comparison between the calibration equations obtained with routine SAND 1 (blue and red curves) and the one published by Vardy et al. (2007) using the routine FINE 1 (grey curve).

### 3.2.2 Step 2: Methodology proposed by Grabowski et al. (2010) to estimate CSS from the CSM erosion threshold

The second step consists in estimating the critical shear stress from the stagnation pressure previously calculated at the erosion threshold. The methodology to achieve this was proposed by Grabowski et al. (2010). They compared erosion thresholds given by the CSM and a laboratory annular flume for different sediment mixtures of fine quartz sand ( $d_{50}= 224 \mu\text{m}$ ) and kaolin clay contents varying between 5% to 35% (Figure 15). Water content of sediment mixtures was maintained at 25% during all tests.

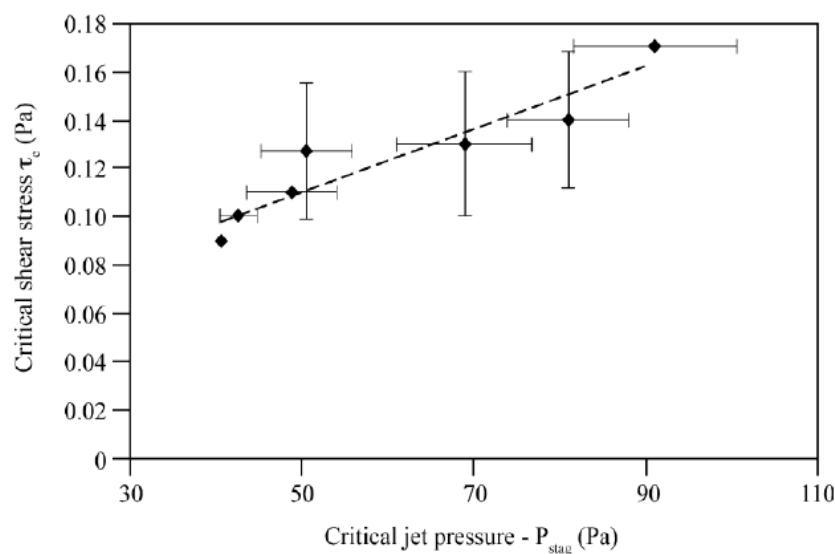


Figure 15: Correlation between the mean critical shear stress ( $\tau_c$ ) estimated by the annular flume and the mean critical jet stagnation pressure ( $P_{stag}$ ) estimated with the CSM (Grabowski et al. 2010). Error bars are standard error between the five replicates taken for each sediment mixture.

The relationship obtained by Grabowski et al. (2010) between the mean critical shear stress ( $\tau_c$ ) estimated by the annular flume and the mean critical jet stagnation pressure assessed by the CSM is given by Equation 4 and is used as calibration equation in this study.

$$\tau_c = 0.0013P_{stag} + 0.047 \quad (R^2 = 0.87, P < 0.01) \quad (4)$$

It should be noted that this calibration only applies to erosion thresholds obtained using the routine SAND 1 and for calculated stagnation pressures between 40-90 Pa which represents the range tested during their study. The authors recommend to researchers using other CMS routines to develop their own calibration equation using the previous methodology.

### 3.2.3 Example of critical shear stress $\tau_c$ calculation

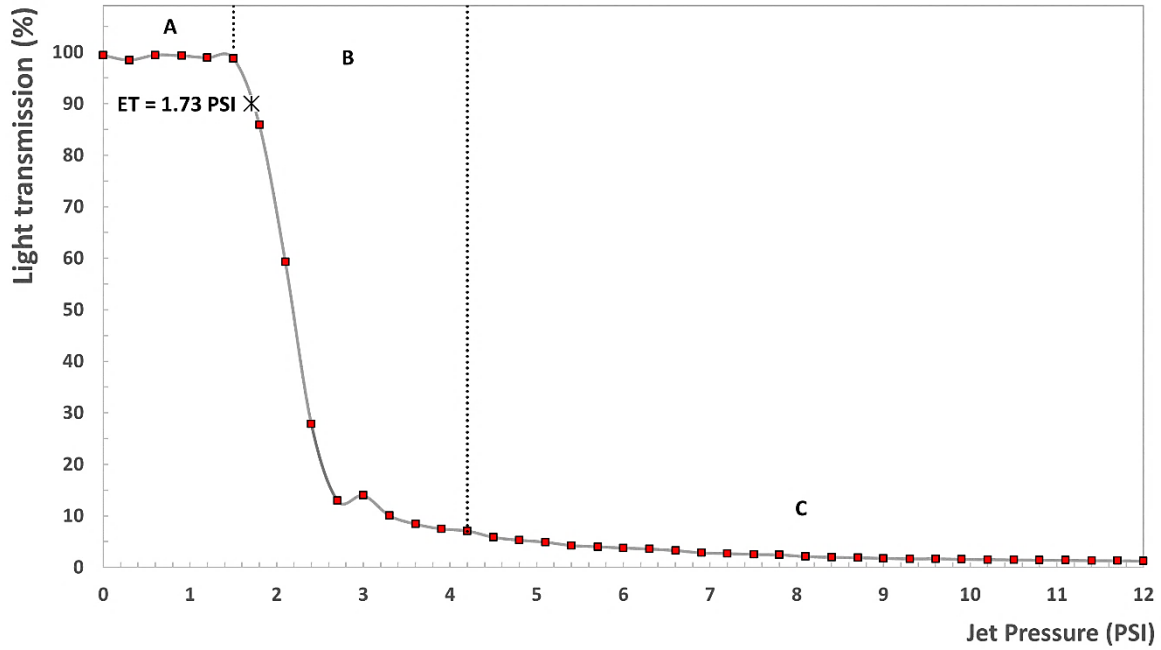


Figure 16: Erosion profile obtained with the CSM on an unfrozen sample (+1.9°C).

On Figure 16, the erosion threshold for an unfrozen silt loam sample occurred at a CSM jet pressure of 1.73 PSI. From Equation 3, we obtained for this soil sample a stagnation pressure  $P_{stag}$  of 179.6 Pascal and from Equation 4 a critical shear stress of 0.28 Pascal.

$$P_{stag} = 94.06x^{1.18} = 94.06(1.73 \text{ PSI})^{1.18} = 179.6 \text{ Pa}$$

$$\tau_c = 0.0013P_{stag} + 0.047 = 0.0013(177.15 \text{ Pa}) + 0.047 = 0.28 \text{ Pa}$$

According to the table of erodibility classes published by Bones (2014), the silt loam of this study would fall in the critical shear stress range of the very erodible class.

Table 2: Shear stress ranges for each erodibility class (Bones, 2014)

Erodibility Class	Critical Shear Stress Range (Pa)
Very Erodible	0.11-0.499
Erodible	0.5-3.49
Moderately Resistant	3.5-7.79
Resistant	7.8-20.99
Very Resistant	$\geq 21.00$

## 4 Results

### 4.1 Critical shear stress

Calculated critical shear stress according to soil temperature is illustrated on Figure 17. No noticeable difference was found between the soil samples consolidated at 10 and 50 kPa and therefore the results were combined during the analysis. The mean  $\tau_c$  for soil samples above 0°C is 0.28 Pascal while the mean  $\tau_c$  for partially frozen soils is 0.27. Results obtained with the CSM device show that even frozen, the soil in the temperature range 0 to -2°C exhibits a similar erosion threshold than if the ground was unfrozen. This means that ice and unfrozen water content present between soil grains does not provide the necessary bonding to increase erosion resistance as generally thought. As soon as the soil temperature falls below -2°C, the relation between  $\tau_c$  and soil temperature become linear and negatively correlated. For every soil degree temperature decrease, there is a 1.6 increase in magnitude of CSS. Below -2°C, erodibility appears to be more influenced by heat transfer between water and the soil. On Figure 17, the horizontal gray line delimits the erodibility classes provided by Bones (2014) in Table 5. Below -3°C, the soil moves from a the very erodible class to the erodible.

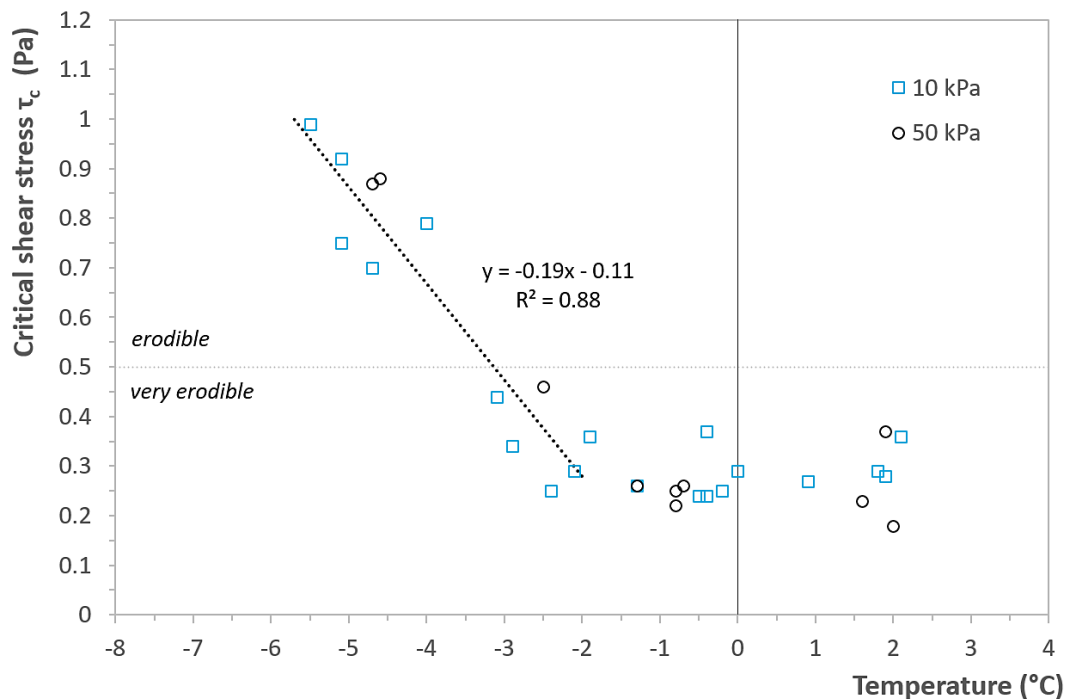


Figure 17: Critical shear stress of the Røros silt loam according to soil temperature.

Table 4 shows the jet pressure, stagnation pressure and critical shear stress measured for every test according to the degree of consolidation and the soil temperature. Mean jet pressures

measured with the CSM, mean calculated stagnation pressures  $P_{stag}$  and mean critical shear stresses  $\tau_c$  are given in Table 3 for unfrozen and partially frozen soil samples along with relationships obtained for the frozen soil samples. In the study of McCool et al. (2013), they also obtained a similar trend of  $\tau_c$  at their study site for non-frozen and thawing soils in winter with respective values of 0.80 to 0.77 Pascal while for the frozen ground the mean value was 1.16 Pascal.

*Table 3: Jet pressures, stagnation pressures and critical shear stresses according to the degree of consolidation and the soil temperature.*

<b>Consolidation (kPa)</b>	<b>Soil temperature (°C)</b>	<b>Jet pressure (PSI)</b>	<b>Jet pressure at soil surface <math>P_{stag}</math> (Pa)</b>	<b><math>\tau_c</math> (Pa)</b>
10	-5.5	5.64	724.29	0.99
10	-5.1	4.42	543.25	0.75
10	-5.1	5.30	673.05	0.92
10	-4.7	4.14	502.88	0.7
10	-4.0	4.60	569.45	0.79
10	-3.1	2.92	333.09	0.44
10	-2.9	2.00	225.75	0.34
10	-2.4	1.51	152.97	0.25
10	-2.1	1.82	190.67	0.29
10	-1.9	2.23	242.33	0.36
10	-1.3	1.60	163.78	0.26
10	-0.5	1.46	147.01	0.24
10	-0.4	2.28	248.75	0.37
10	-0.4	1.47	149.39	0.24
10	-0.2	1.53	155.36	0.25
10	0	1.82	190.68	0.29
10	0.9	1.65	169.84	0.27
10	1.8	1.81	189.44	0.29
10	1.9	1.71	177.15	0.28
10	2.1	2.19	237.21	0.36
50	-4.7	5.05	635.75	0.87
50	-4.6	5.07	638.73	0.88
50	-2.5	2.78	314.32	0.46
50	-1.3	1.63	167.41	0.26
50	-0.8	1.33	131.69	0.22
50	-0.8	1.53	155.35	0.25
50	-0.7	1.61	165	0.26
50	1.6	1.39	138.73	0.23
50	1.9	2.28	248.75	0.37

50	2.0	1.09	104.13	0.18
----	-----	------	--------	------

Table 4: Mean values and relationships of jet pressures, stagnation pressures and critical shear stress according to the soil thermal state.

	$P_{jet}$ (PSI)	$P_{stag}$ (Pa)	$\tau_c$ (Pa)
<b>Unfrozen</b>	1.69	174.2	0.28
<b>Partially frozen (0 to -2°C)</b>	1.66	170.9	0.27
<b>Frozen (-2 to -6°C)</b>	(9) $P_{jet} = -1.08T - 0.37$	(10) $P_{stag} = -148.8T - 114.3$	(11) $\tau_c = -0.19T - 0.11$

## 4.2 Erosion scour

Figure 18 presents examples of erosion scours observed for the 3 soil thermal states (i.e. frozen, partially frozen and unfrozen) at the end of the 2 minutes CSM test. The shape of erosion scour was found to be different between unfrozen (Figure 18A) and frozen soil samples (Figure 18C). The scour is a well-defined circular hole, narrower and deeper when the soil was unfrozen while it was shallower and wider when frozen. For the partially frozen soil samples, the scours had an irregular shape and looked like a mix between unfrozen and frozen scours (Figure 18B). Mean scour dimensions are presented in Table 5. The volume was estimated using the equation for a half ellipse. This resulted in the scour volume for partially frozen ground being highest and lowest for frozen ground. The temperature measured in the middle of the erosion scours at the end of testing was ranging between -0.3°C to 0.2°C for the samples that were previously frozen.

Table 5: Mean scour surface area, depth, and volume according to soil temperature.

	Temperature (°C)		
	> 0	0 to -2	< -2
Mean scour surface area (cm <sup>2</sup> )	1.1	1.7	1.6
Mean scour depth (cm)	0.4	0.3	0.2
Mean scour volume (cm <sup>3</sup> )	0.83	1.00	0.65

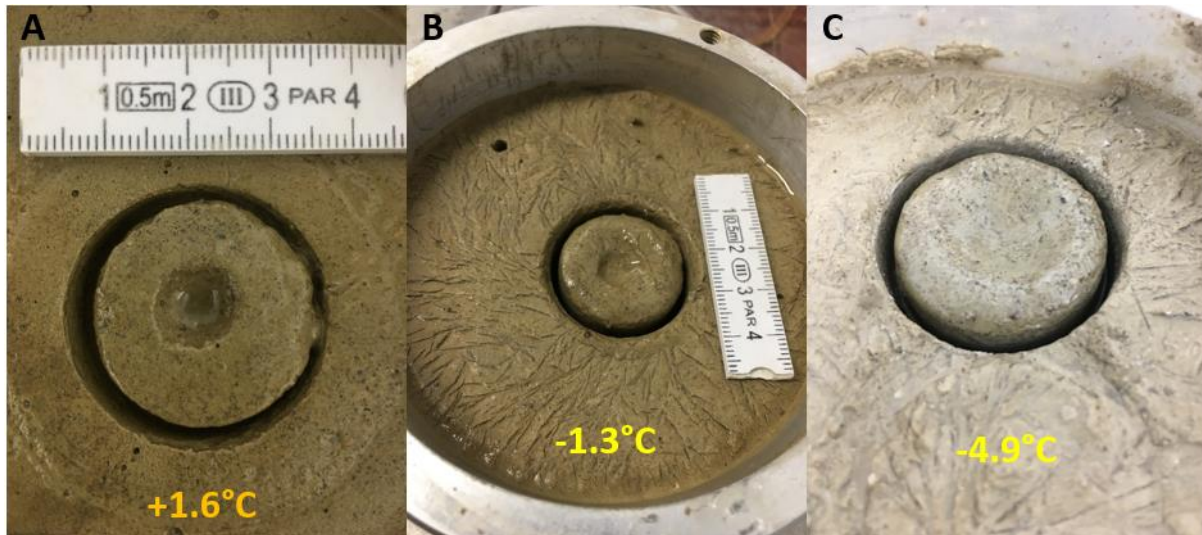


Figure 18: Scour of erosion observed for the 3-soil thermal states at the end of the CSM test.

## 5 Data validation with other laboratories studies

Grabowski et al. (2010) stated that their CSS calibration (Equation 4) should only be used for the range of stagnation pressures tested i.e. between 40-90 Pa. However, most of stagnation pressures  $P_{stag}$  calculated during this study are above 90 Pa (Table 4). Nevertheless, it was found that the CSS results obtained for the unfrozen soil samples show good similitudes with other studies using the same type of soil. Here are some examples.

### *Wang 2013*

Values reported from the literature of critical shear stress varying with bulk density was plotted by Wang (2013). Even though the data shown on Figure 19 were obtained using different erosion devices and different cohesive sediment types, an increase in critical shear stress as sediment bulk density increases is observed.

In this study, for the unfrozen silt loam from Røros, the average measured wet bulk density after a 10 kPa consolidation was 2057 kg/m<sup>3</sup> and the average CSS value was 0.3 Pascal. The yellow dot on Figure 19 shows the location corresponding to these two values. It is possible to deduce from the plot that the data from this study fall within the range of possible values previously published in the literature.

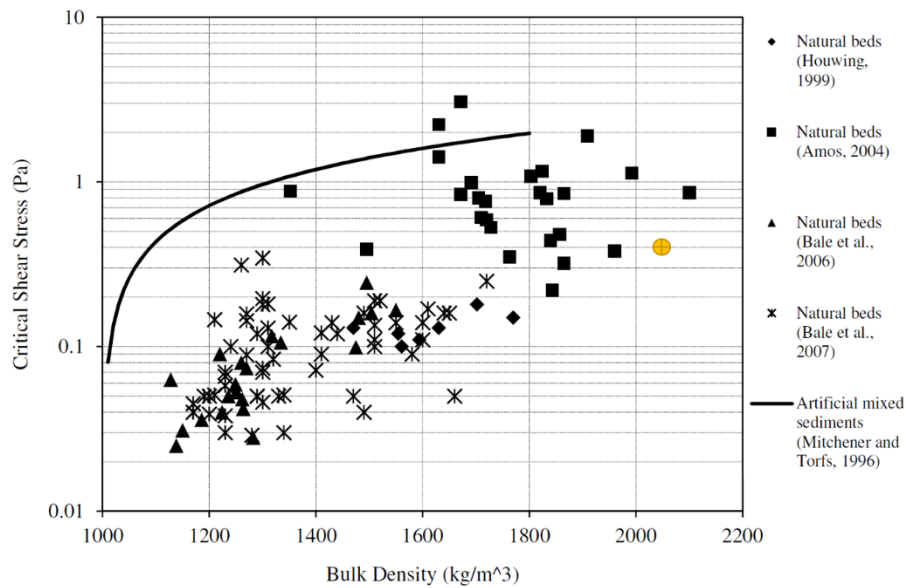


Figure 19: Critical shear stress according to bulk density reported from the literature for different cohesive sediments (modified from Wang 2013). The yellow dot refers to the silt from Røros.

### Thomsen and Gust 2000

CSS of continental margin sediments from the Celtic Sea were obtained with the aid of a circular laboratory erosion chamber using a rotating plate. The silty sediments tested contained 15-40% of particles  $< 63 \mu\text{m}$ . The relationship between CSS and particle size of unconsolidated and consolidated marine sediments taken at different seabed sites is illustrated on Figure 20. This graph gives us a CSS value of 0.2 Pascal for the consolidated silt loam from Røros having a median particle size of  $29 \mu\text{m}$ .

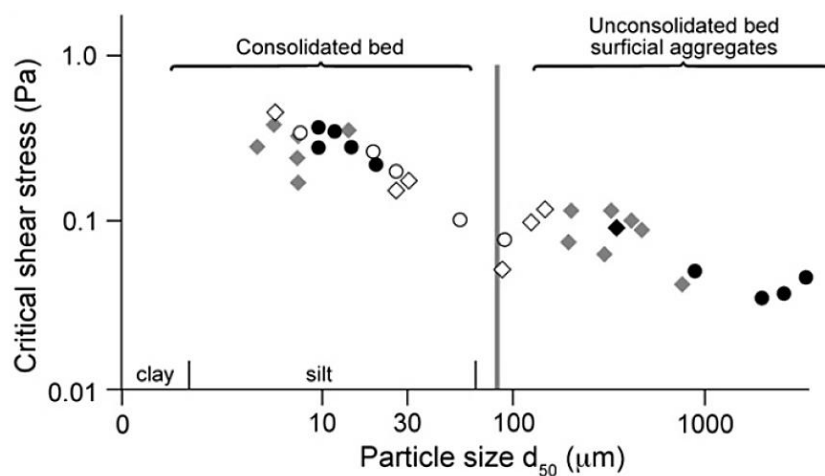


Figure 20: Critical shear stress according to particle size of unconsolidated and consolidated marine sediment. Symbols represent different study sites (after Thomsen and Gust 2000 in Grabowski et al. 2011).

**Perkey, Smith and Priestas 2020**

One part of their laboratory experiment consisted in mixing a fine sand (125–250  $\mu\text{m}$ ) with varying kaolinite contents between 0 to 100%. The relationship found between CSS and kaolinite contents using the U.S. Army Corps of Engineers Sedflume erosion device is shown in Figure 21. Sedigraph grain size data for the kaolinite was given to be >98% clay (< 4  $\mu\text{m}$ ). According to the grain size distribution of Figure 4, the Røros silt has 7% of soil particles smaller than 4  $\mu\text{m}$  which refers to a CSS value of 0.29 Pascal on Figure 21 (red line), which is exactly within the value range obtained as part of this study.

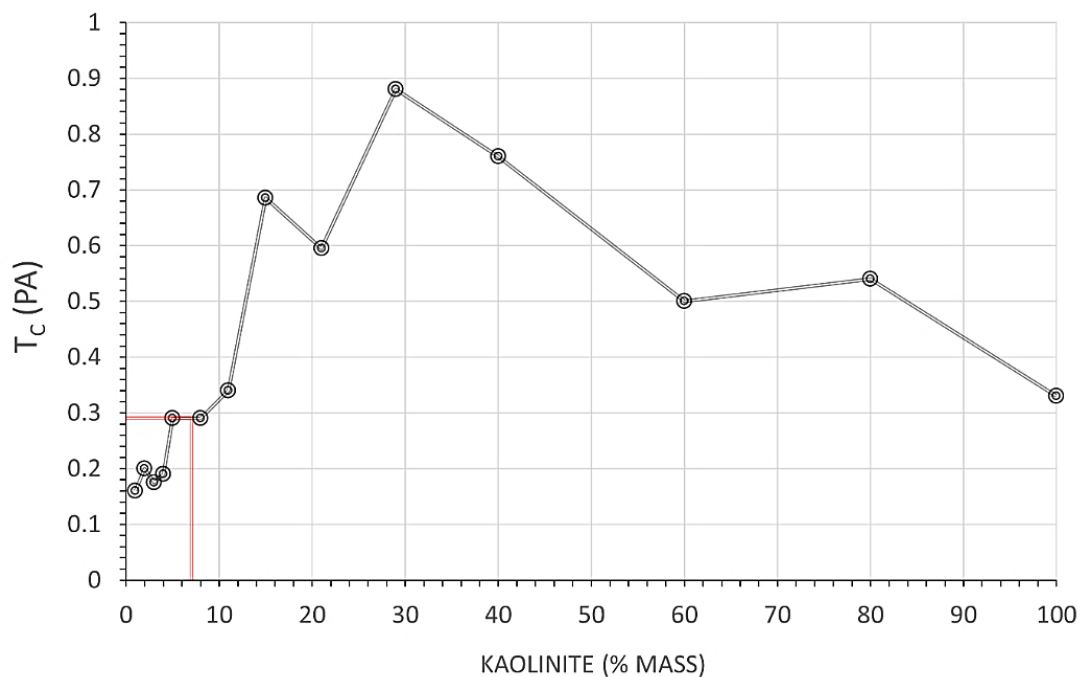


Figure 21: Critical shear stress  $\tau_c$  plotted against kaolinite content (After Perkey et al. 2020).

## 6. Conclusion

It is generally believed that frozen ground cannot be easily eroded since ice add additional bonding between soil grains and increase strength as soon as the soil falls below 0°C. However, the results obtained in this study showed that this bonding start to be effective against erosion only from -2°C for a silty soil. For colder temperatures than -2°C, the critical shear stress at which soil particles will be remove will not correspond to a single value but will be a function of temperature. From -2°C to -6°C, the cohesive shear stress of the Røros silt increased by a factor of 1.6 for every degree Celsius decrease. The mean CSS measured in the laboratory for soil samples above 0°C is 0.28 Pascal while the mean CSS for partially frozen soils is 0.27 Pascal, meaning that in both cases erosion starts under the same hydraulic stress. Those CSS values relate to the very erodible class of sediment.

No significant difference in CSS was observed between the two consolidation levels at 10 and 50 kPa. However, it is to be expected that for clay soils, the response to consolidation and erosion should be different. Grabowski et al. (2010) observed that a minimum clay content of 5% is needed for a sand/clay mixture to be cohesive. In the same way, it would be interesting to evaluate the erosion resistance of a silt by adding different clay contents. There is also a need to continue the calibration between the cohesive strength meter and a flume as proposed by Grabowski et al. (2010) for higher stagnation pressures as well as for the other routines provided by the cohesive strength meter.

To conclude, soils in cold regions are experiencing increased hydraulic and thermal forcing due to climatic changes such as intensification of winter precipitation and increased freeze-thaw cycles. The applicability of the cohesive strength meter to frozen soils brought a better understanding on erosion resistance of silty soils and showed the importance of separating frozen ground into distinct thermal states when analyzing CSS data (i.e. frozen, partially frozen and unfrozen/thawed). The approach described in this research is innovative. To our knowledge it is the first time the cohesive shear stress of a frozen silt is assess according to different freezing temperatures. The results obtained have therefore a high potential of application in cold regions science and engineering.

## References

- Aviles, D., Berglund, K. Wesstrom, I. Joel, A. 2020. Effect of liming products on soil detachment resistance, measured with a cohesive strength meter, ACTA AGRICULTURAE SCANDINAVICA, SECTION B — SOIL & PLANT SCIENCE, 2020, VOL. 70, NO. 1, 48-55. <https://doi.org/10.1080/09064710.2019.1668475>
- Bones, E. 2014. Predicting critical shear stress and soil erodibility classes using soil properties. Master Thesis, Georgia Institute of Technology, 127 pp.
- Edwards, L. M. and Burney, J. R. (1987). Soil erosion losses under freeze/thaw and winter ground cover using a laboratory rainfall simulator. *Canadian Agricultural Engineering* 29, 109-115.
- Ferrick M. G. and Gatto L.W. 2005. Quantifying the effect of a freeze–thaw cycle on soil erosion: laboratory experiments, *Journal of Earth Surface Processes and Landforms* 30: 1305-1326. DOI:10.1002/esp.1209
- Flerchinger, G.N., Lehrsch, G.A. McCool D.K (2005). Freezing and thawing | Processes, *Encyclopedia of Soils in the Environment*, 2005, Pages 104-110, <https://doi.org/10.1016/B978-0-12-409548-9.05173-3>
- Friend, P.L., Lucas, C.H., Rossington, S.K. (2005). Day–night variation of cohesive sediment stability, *Journal of Estuarine, Coastal and Shelf Science*, Volume 64, Issue 2-3, 407-418.
- Friend, P.L., Lucas, C.H. and Rossington, S.K. 2005. Day-night variation of cohesive sediment stability, *Estuarine, Coastal and Shelf Science*, 64 (2–3): 407-418. doi:10.1016/j.ecss.2005.03.006
- Froese, J.C., R.M.Cruse, and M.Ghaffarzadeh. 1999. Erosion mechanics of soils with an impermeable subsurface layer. *Soil Science Society of America Journal* 63:1836–1841. doi:10.2136/sssaj1999.6361836x.
- Grabowski, R. C., 2014. Measuring the shear strength of cohesive sediment in the field. In Cook SJ, Clark LE, and Nield JM (eds), *Geomorphological Techniques*. British Society for Geomorphology, Part 1, Sec. 3.1, 1-7.
- Grabowski, R.C., Wharton, G., Davies, G. R., and Droppo, I.G. 2012. Spatial and temporal variations in the erosion threshold of fine riverbed sediments, *Journal of Soils Sediments* 12:1174-1188. DOI 10.1007/s11368-012-0534-9.
- Grabowski, R.C., Droppo, I.G. & Wharton, G. 2011. Erodibility of cohesive sediment: The importance of sediment properties. *Earth-Science Reviews* 105 (3-4): 101-120. <https://doi.org/10.1016/j.earscirev.2011.01.008>

- Grabowski, R.C., Droppo, I.G. & Wharton, G. 2010. Estimation of critical shear stress from cohesive strength meter-derived erosion thresholds. *Limnology and Oceanography-Methods* 8: 678-685.
- Guegan, E. 2016. Cohesive Strength Meter: Applicability to frozen (thawing) soils. Report submitted to the Sustainable Arctic Marine and Coastal Technology SAMCoT WP6 research group from the Norwegian University of Science and Technology NTNU, Trondheim, Norway, 13 pp.
- Henshaw, A. J. Thorne, C. R. and Clifford, N. J. 2012. Identifying causes and controls of river bank erosion in a British upland catchment, *Journal of Catena*, 100:107-119, <https://doi.org/10.1016/j.catena.2012.07.015>.
- Lawler, D. M. 1992. Process dominance in bank erosion, In book: *Lowland Floodplain Rivers: Geomorphological Perspectives*, Publisher: John Wiley and Sons Ltd, Editors: Paul Carling, Geoff Petts, Chapter 5: 117-143.
- Lawler, D. M. 1986. River bank erosion and the influence of frost; a statistical examination, *Transactions of the Institute of British Geographers*, 11 (1986), pp. 227-242
- Lee, J. H.W. and Chu, V. H. 2003. *Turbulent Jets and Plumes: A Lagrangian Approach*, Springer Science + Business Media New York, Volume 1:408 pp.
- Leopold, L. B. 1973. River channel change with time: an example. *Geological Society of America Bulletin*, 84, 1845-1860.
- Liu, H., Yang, Y., Zhang, K. and Sun, C. 2017. Soil erosion as Affected by freeze-thaw regime and Initial Soil moisture Content, *Soil Science Society of America Journal* 81:459-467.
- Loranger B. 2020. Laboratory investigation of frost susceptibility of crushed rock aggregates and field assessment of frost heave and frost depth. Doctoral thesis. Department of Civil and Environmental Engineering, Norwegian University of Science and Technology, 2020:335. <https://hdl.handle.net/11250/2686021>
- McCool, D. K., Dun, S., Wu J. Q., Elliot W. J., and Brooks E. S. 2013. Seasonal change of WEPP erodibility parameters for two fallows plots on a Palouse Silt Loam, *American Society of Agricultural and Biological Engineers*, 56(2): 711-718.
- PARTRAC 2011. Cohesive Strength Meter MK IV Operating Manuel, P.0006.02.05.D001v04, Glasgow, UK, 25pp.
- Paterson, D. M. (1989). Short term changes in the erodibility of intertidal cohesive sediments related to the migratory behaviour of epipellic diatoms. *Limnology and Oceanography*, 34(1), 223-234. <https://doi.org/10.4319/lo.1989.34.1.0223>

- Perkey, D. W., Smith, J.S., and Priestas, A.M. (2020). Erosion thresholds and rates for sand-mud mixtures. Final Technical Report ERDC/CHL TR-20-13, US Army Engineer Research and Development Center, Vicksburg, MS, USA, 84 pp.
- Stott, T. 1997. A comparison of stream bank erosion processes on forested and moorland streams in the balquhider catchments, Central Scotland, *Earth surface processes and landforms* 22: 383-399. [https://doi.org/10.1002/\(SICI\)1096-9837\(199704\)22:4<383::AID-ESP695>3.0.CO;2-4](https://doi.org/10.1002/(SICI)1096-9837(199704)22:4<383::AID-ESP695>3.0.CO;2-4)
- Sun B., Ren F., Ding W., Zhang G., Huang J., Li J., Zhang L. 2021: Effects of freeze-thaw on soil properties and water erosion. *Soil & Water Research*, 16: 205–216. <https://doi.org/10.17221/143/2020-SWR>
- Thomsen, L. and Gust, G. 2000. Sediment erosion thresholds and characteristics of resuspended aggregates on the western European continental margin, *Deep-Sea Research Part I—Oceanographic Research Papers*, 47 (10): 1881-1897. [https://doi.org/10.1016/S0967-0637\(00\)00003-0](https://doi.org/10.1016/S0967-0637(00)00003-0).
- Tolhurst T. J., Black K. S., Shayler S. A., Mather S., Black I., Baker K. and Paterson D. M. (1999). Measuring the in situ erosion shear stress of intertidal sediments with the cohesive strength meter (CSM), *Estuarine, Coastal and Shelf Science* 49(2), 281–294. <https://doi.org/10.1006/ecss.1999.0512>.
- Van Klaveren, R. W., and D. K. McCool. 2010. Freeze-thaw and water tension effects on soil detachment. *Soil Science Society of America* 74(4): 1327-1338. doi:10.2136/sssaj2009.0360.
- Vardy S, Saunders JE, Tolhurst TJ, Davies PA, Paterson DM. 2007. Calibration of the high-pressure cohesive strength meter (CSM). *Continental Shelf Research* 27(8): 1190-1199. DOI:10.1016/j.csr.2006.01.022
- Wang, Y. C. 2013. Effects of physical properties and rheological characteristics on critical shear stress of fine sediments, PhD dissertation, Georgia Institute of Technology, 270pp.
- Widdows J., Friend, P.L. Bale, A.J., Brinsley, M.D., Pope, N.D. and Thompson, C.E.L. 2007. Inter-comparison between five devices for determining erodability of intertidal sediments, *Journal of Continental Shelf Research*, Volume 27, Issue 8, 1174-1189. doi:10.1016/j.csr.2005.10.006
- Wolman, G.M. 1959. Factors influencing erosion of a cohesive riverbank, *American Journal of Science*, 257 (3) 204-216, DOI: <https://doi.org/10.2475/ajs.257.3.204>

- Yallop, M., Paterson, D. & Wellsbury, P. 2000. Interrelationships between Rates of Microbial Production, Exopolymer Production, Microbial Biomass, and Sediment Stability in Biofilms of Intertidal Sediments 39: 116–127. <https://doi.org/10.1007/s002489900186>.
- Yallop, M. L., de Winder B. Paterson D. M. and Stal, L. J. 1994. Comparative structure, primary production and biogenic stabilization of cohesive and non-cohesive marine sediments inhabited by microphytobenthos, *Journal of Estuarine, Coastal and Shelf Science*, Volume 39, Issue 6, 565–582. [https://doi.org/10.1016/S0272-7714\(06\)80010-7](https://doi.org/10.1016/S0272-7714(06)80010-7).
- Yen, E. S. and Molnau, M. 1982. Frozen soil effects on the erosion hazard, Idaho Water and Energy Resources Research Institute, Report Project A-070-IDA, 66 pp. <https://www.lib.uidaho.edu/digital/iwdl/docs/iwdl-198212.htm>.
- Yumoto et al., 2006, M. Yumoto, T. Ogata, N. Matsuoka, E. Matsumoto, Riverbank freeze-thaw erosion along a mountain stream, Nikko volcanic area, central Japan, *Permafrost and Periglacial Processes*, 17 (2006), pp. 325-339
- Zuzel, J.F., Allmaras R.R., and Greenwalt R. 1982. Runoff and soil-erosion on frozen soils in Northeastern Oregon. *Journal of Soil and Water Conservation*, 37(6):351–354.